nature climate change

ARTICLES

https://doi.org/10.1038/s41558-020-00963-x

Check for updates

Zonally contrasting shifts of the tropical rain belt in response to climate change

Antonios Mamalakis[1]✉, James T. Randerson[2], Jin-Yi Yu[2], Michael S. Pritchard[2], Gudrun Magnusdottir[2], Padhraic Smyth[3,4], Paul A. Levine[2], Sungduk Yu[5] and Efi Foufoula-Georgiou[1,2]✉

Future changes in the position of the intertropical convergence zone (ITCZ; a narrow band of heavy precipitation in the tropics) with climate change could affect the livelihood and food security of billions of people. Although models predict a future narrowing of the ITCZ, uncertainties remain large regarding its future position, with most past work focusing on zonal-mean shifts. Here we use projections from 27 state-of-the-art climate models and document a robust zonally varying ITCZ response to the SSP3-7.0 scenario by 2100, with a northward shift over eastern Africa and the Indian Ocean and a southward shift in the eastern Pacific and Atlantic oceans. The zonally varying response is consistent with changes in the divergent atmospheric energy transport and sector-mean shifts of the energy flux equator. Our analysis provides insight about mechanisms influencing the future position of the tropical rain belt and may allow for more-robust projections of climate change impacts.

The intertropical convergence zone (ITCZ) and its dynamics[1] play a vital role in the tropical atmospheric circulation and hydroclimate, sustaining tropical forest and savanna ecosystems, and influencing the livelihoods of billions of people. As such, intense research has focused on identifying the physical mechanisms that determine the climatology and variability of the ITCZ position on intra-seasonal to interannual scales[1–10] and its long-term response to large-scale natural climate variability and anthropogenic forcing[1,5,11–23].

Past studies have shown that perturbations in the interhemispheric asymmetry of the net energy input into the atmosphere will shift the ITCZ towards the more-heated hemisphere[1]. For example, projected reductions in aerosol emissions[24–26], Arctic sea-ice loss (related to Arctic amplification[27,28]) and glacier melting in the Himalayas[29,30] will reduce albedo significantly more in the Northern Hemisphere than in the Southern Hemisphere, resulting in northern heating and an ITCZ shift to the north[18,22,31]. By contrast, the Atlantic meridional overturning circulation (AMOC) is expected to weaken in the future[32–35] (new results indicate that it has already been weakening[36]), which will result in a reduction of the northward oceanic heat transport from the tropics to the northern Atlantic and a northern cooling, leading to a southward shift of the ITCZ[22,37,38].

Despite the relative consensus in the literature with regard to the zonal-mean response of the ITCZ location to individual forcing agents as discussed in the preceding paragraph, there is still high uncertainty regarding the response of the ITCZ location to the integrated effect of all these processes under climate change. This uncertainty stems mainly from different model physics that yield different responses even to identical climate change scenarios. Specifically, although a future narrowing of the ITCZ is a robust projection expected with climate change[20], models differ considerably regarding changes in the position of the ITCZ, yielding to an almost zero zonal-mean ITCZ shift when considering the multimodel mean[22]. Another reason for this uncertainty is that most studies have focused on zonal-mean changes of the ITCZ, possibly masking model agreement over shifts in particular longitudinal sectors. Indeed, because of the compensating effects of the relevant radiative and dynamical processes influencing the ITCZ position, and since most of these processes are not expected to be equally influential in different longitudinal sectors, the integrated ITCZ response to climate change should not be expected to be homogeneous in longitude[18]. Thus, exploring the longitudinally explicit changes of the ITCZ location is necessary to gain insight into its future response and to identify robust model projections across different longitudinal sectors.

In this article, we explore the ITCZ response to climate change during the twenty-first century using 1983–2005 as a base period and comparing with projections during 2075–2100. In our analysis, we use Earth system model simulations from the sixth phase of the Coupled Model Intercomparison Project[39] (CMIP6; a total of 27 different models and 105 individual runs; Supplementary Table 1) forced with the combination of the Shared Socioeconomic Pathway 3 (SSP3) and the Representative Concentration Pathway 7.0 (RCP 7.0) scenario[40,41]. For each model simulation, we estimate seasonal and annual-mean changes of the ITCZ position as a function of longitude (in 1° increments), while also considering the effect of the models' present-day ITCZ biases on the revealed changes. Given the existing ambiguity in the literature as to a regional ITCZ definition[42], we clarify that for the purposes of this study, the position of the ITCZ is defined as the latitude of maximum (above a specific quantile) precipitation and minimum outgoing longwave radiation (OLR) in each longitude, using a probabilistic approach[43] (Methods). For the sake of completeness, we also present results based on simpler, univariate precipitation or OLR indices/maps to assess ITCZ changes. We acknowledge that the adopted tracking approaches might be masking inherent differences in regional precipitation features (for example, land versus oceanic rain belts);

[1]Department of Civil and Environmental Engineering, University of California, Irvine, CA, USA. [2]Department of Earth System Science, University of California, Irvine, CA, USA. [3]Department of Computer Science, University of California, Irvine, CA, USA. [4]Department of Statistics, University of California, Irvine, CA, USA. [5]Department of Geology and Geophysics, Yale University, New Haven, CT, USA. ✉e-mail: amamalak@uci.edu; efi@uci.edu

Table 1 | Multimodel mean and intermodel standard deviation of future ITCZ and EFE shifts (2075–2100 minus 1983–2005; positive values indicate northward movement) and changes of the inter-hemispheric energetic asymmetry over different longitudinal sectors, as obtained from 27 CMIP6 model outputs

		Global zonal mean	Eurasian sector (20° E–130° E)	East Pacific–Atlantic sector (110° W–0°)
ITCZ latitude (° N)	Base period	**3.6 ± 2.0**	**−1.0 ± 1.1**	**4.1 ± 2.3**
	Future shift	−0.5 ± 1.2	**0.8 ± 0.6**	**−0.7 ± 0.9**
$Q_S - Q_N$ (PW)	Base period	−0.03 ± 0.37	**0.93 ± 0.21**	**−0.96 ± 0.23**
	Future change	−0.05 ± 0.21	**−0.24 ± 0.10**	**0.31 ± 0.16**
EFE latitude (° N)	Base period	−0.3 ± 1.1	**−3.5 ± 0.8**	**4.4 ± 2.2**
	Future shift	0.0 ± 0.6	**0.6 ± 0.4**	**−1.3 ± 1.2**
EFE latitude approximation[10] (° N)	Base period	−0.4 ± 0.8	**−3.3 ± 0.9**	**4.5 ± 1.7**
	Future shift	0.2 ± 0.5	**0.7 ± 0.4**	**−1.3 ± 1.0**

The baseline values (referring to 1983–2005) are also provided. Values with bold font correspond to a multimodel mean that is statistically distinguishable from zero on the basis of the *t* test ($P < 0.01$). It is shown that there is a robust consensus across models regarding future changes in the Eurasian and eastern Pacific–Atlantic sectors, but such a consensus is not apparent in the global zonal mean. Note, for example, that in the sector-mean analysis, the intermodel variability (standard deviation) in future changes is either smaller than or of the same magnitude as the multimodel mean, while in the global zonal-mean analysis, the intermodel variability is in all cases two to four times larger than the multimodel mean.

however, such detailed phenomenology and attribution is not the focus in this study.

We provide evidence that models exhibit high consensus regarding future ITCZ shifts as a function of longitude despite the large intermodel spread in the zonal-mean response. The ITCZ shifts are evaluated for physical consistency with future changes in equatorial sea surface temperature (SST), as well as changes in the horizontal atmospheric energy transport (AET) and associated shifts in the energy flux equator (EFE).

Future zonally contrasting shifts of the ITCZ

The annual and zonal-mean ITCZ shift during the twenty-first century for the CMIP6 models is −0.5 ± 1.2° N (a small southward shift; Table 1). The intermodel spread within the CMIP6 models is very large (the standard deviation is more than twice the mean shift), which leads to the multimodel mean shift not being statistically distinguishable from zero, and confirming previous reports[22,44].

Despite the high intermodel uncertainty regarding the zonal-mean ITCZ shift, the CMIP6 models show greater agreement for different longitudinal sectors (see Fig. 1 and Methods for information on the tracking approach of the ITCZ; explanatory schematics are provided as Supplementary Figs. 1 and 2). For the May–October season, the models exhibit a robust northward shift of the ITCZ over eastern/central Africa and the Indian Ocean and a southward shift over most of the Pacific and Atlantic oceans (Fig. 1a). The projected shift over the Indian Ocean comes primarily from a northward shift in the near-equatorial precipitation (which represents a secondary ITCZ feature in the present-day observations during this season that is physically linked with the so-called equatorial jump[45,46]), rather than a shift in the subtropical 'monsoonal' primary convergence zone. The revealed shift has been argued to associate with future increases in SST in the northern Indian Ocean and locally developed Bjerknes feedbacks between SST gradients and wind and thermocline changes in the basin[47]. In the November–April season, the south Indian Ocean convergence zone and the south Pacific convergence zone both shift northward[48], while the eastern Pacific ITCZ is shown to shift southward. In the Atlantic basin, there is an equatorward shift of the ITCZ. In general, zonally distinct (and contrasting) responses of the position of the ITCZ to climate change occur during both seasons, and an even more robust response is visible on annual timescales (Fig. 1c and Table 1). This response consists of a northward shift over eastern Africa and the Indian Ocean and a southward shift over the eastern Pacific Ocean, the Atlantic Ocean and South America (where a less-robust southward shift is shown). The zonally distinct responses are also apparent when calculating the future changes in precipitation or OLR (Supplementary Figs. 3 and 4).

To more precisely quantify the zonally distinct responses of the ITCZ to climate change, we tracked the temporal evolution of the ITCZ location as a function of longitude and over two different longitudinal sectors. We define the Eurasian sector as spanning 20° E–130° E and the eastern Pacific–Atlantic sector as spanning 110° W–0°. We note that the boundaries of these sectors were chosen from visible breaks shown in Fig. 2a, but our results are robust if the boundaries are moderately changed (that is, by ±10° of longitude). A northward ITCZ shift occurs for the Eurasian sector, while a southward shift occurs in the eastern Pacific–Atlantic sector (Fig. 2a). Over the western Pacific, the ITCZ shifts southward during May–October and northward during November–April (Fig. 1), which translates into a decreased seasonal ITCZ migration in the future and an annual-mean shift that is nearly zero. When comparing the 2075–2100 and 1983–2005 periods, a statistically significant (using the *t* test; $P < 0.01$) northward shift on the order of 0.8 ± 0.6° is obtained over the Eurasian sector (Table 1). By contrast, over the eastern Pacific–Atlantic sector, CMIP6 models indicate a statistically significant southward shift on the order of 0.7 ± 0.9°. The future ITCZ shift and the corresponding change in annual-mean tropical precipitation asymmetry (change in the quantity: $\mathrm{Precip}_{0°–20° N} - \mathrm{Precip}_{0°–20° S}$) between the periods 2075–2100 and 1983–2005 are shown for every CMIP6 model in Fig. 2b, indicating that the majority of models predict a future increase in precipitation in the northern subtropics relative to the south over the Eurasian sector (red colour). The opposite is true for most CMIP6 models over the eastern Pacific–Atlantic sector (blue colour). Figure 2b also shows the robustness of the zonally distinct ITCZ responses with respect to using different indicators to assess changes in the ITCZ position; both the precipitation asymmetry and the ITCZ tracking method yield consistent estimates for most CMIP6 models.

To gain insight about the impact of model biases on our interpretation of the future ITCZ shifts, we have calculated the present-day double-ITCZ biases for each model and over each basin, and then regressed the obtained biases with the future ITCZ shifts (Methods and Supplementary Discussion). We find that the double-ITCZ biases, if anything, are obscuring the full extent of the southward ITCZ shift over the eastern Pacific–Atlantic sector, and thus, our results regarding the zonally contrasting shifts are on the conservative side (Supplementary Discussion and Supplementary Figs. 5–8).

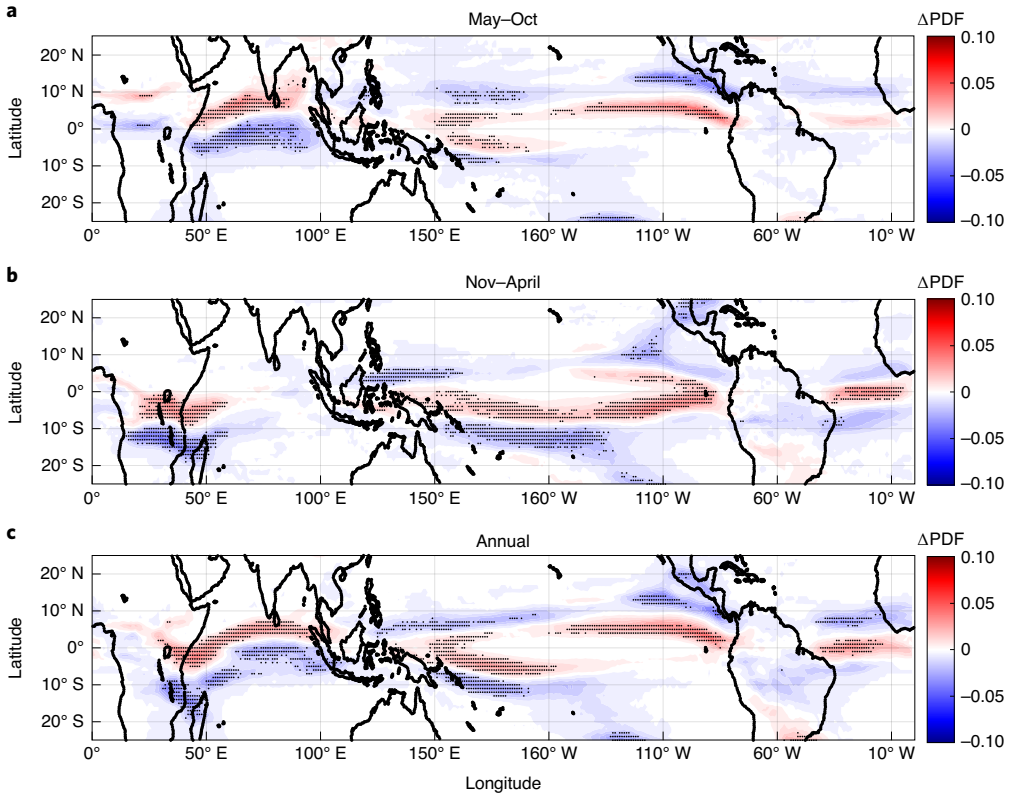

Fig. 1 | Future changes in the location of the ITCZ in response to climate change, as projected by CMIP6 models. a, Difference in the probability density function (ΔPDF) of the location of the ITCZ in May–October between the periods 2075–2100 and 1983–2005. In each period, the location of the ITCZ is defined by tracking the location of maximum precipitation and minimum OLR in overlapping longitudinal windows (we use the joint statistics of the two variables; Supplementary Figs. 1 and 2 and Methods). **b**, Same as in **a**, but for November–April. **c**, Same as in **a**, but the changes in the annual distribution are shown. In all plots, the multimodel mean across 27 CMIP6 models is presented for the SSP3-7.0 scenario; stippling indicates agreement (in the sign of the change) in more than three-fourths of the models considered. Results indicate a robust northward ITCZ shift over eastern Africa and the Indian Ocean and a southward ITCZ shift over the eastern Pacific and Atlantic oceans.

Overall, the agreement between CMIP6 models over these two sectors (Table 1 and Figs. 1 and 2) provides confidence that climate change will lead to contrasting meridional shifts of the ITCZ in the Eurasian and eastern Pacific–Atlantic sectors. As already mentioned, these contrasting responses nearly cancel one another, leading to almost zero ITCZ shift from a zonal-mean perspective (Table 1), confirming the recent literature[22,44].

Regional mechanisms

Motivated by the known close coupling between SST and precipitation in the tropics[47,49,50], we explored the consistency of the revealed zonally contrasting shifts of the ITCZ with changes in SST.

We find that over the tropical Pacific Ocean, SST warming is more pronounced in the east than in the west, which is consistent with the anticipated weakening of the Walker circulation with climate change (Fig. 3a)[47,51]. In both the eastern Pacific and Atlantic oceans, higher SST warming occurs at low latitudes between 10° S and 5° N, which is consistent with this region serving as an attractor for a southward shift of the ITCZ from its current baseline position at 4.1 ± 2.3° N for this sector (Fig. 3c). By contrast, over the Indian Ocean, higher SST warming in the northern subtropics is consistent with the predicted shift of the ITCZ to the north from its current baseline position (Fig. 3b). The pattern of SST change in the Indian Ocean resembles a positive Indian Ocean Dipole (IOD) pattern (with more pronounced warming over the northwestern Indian Ocean and less pronounced warming over the southeastern Indian Ocean), traditionally linked to locally developed Bjerknes feedbacks between SST gradients and wind and thermocline changes in the basin[47,51,52].

Regarding precipitation shifts over land and changes in monsoonal dynamics, studies have shown a future shift of rainfall occurrence from early to late in the rainy season under climate change for most of the individual monsoons[53–55], while in terms of the sign of total precipitation change, large intermodel spreads are reported over specific regions[55]. Despite the reported uncertainties, anticipated changes in regional precipitation are generally consistent with our results presented herein[56–59]. In particular, over South America, a southward shift of the south Atlantic convergence zone under climate change has been reported in observations and in model projections, due to the strengthening of the south Atlantic subtropical high[57,58]. By contrast, over Africa, recent studies have found that intense surface warming over Sahara will deepen the Saharan heat low, making the tropical rain belt migrate seasonally farther to the north and reside there longer[59,60]. This will alter the rainfall seasonality in the south and will yield to an increased rainfall in the north and an average northward shift of the tropical rain belt[59]. Last, projections show that global warming will probably cause an increase in the Indian summer monsoon rainfall (Supplementary Fig. 3a), accompanied by an enhancement of extreme precipitation events[61,62]. Apart from monsoonal changes, a future zonally asymmetric change of rainfall over land has been recently projected on the basis of model simulations and attributed to plant physiological responses to rising CO_2 (ref. [63]).

Atmospheric energetic constraints

Although the projected changes in tropical north–south SST gradients are broadly consistent with the revealed zonally contrasting

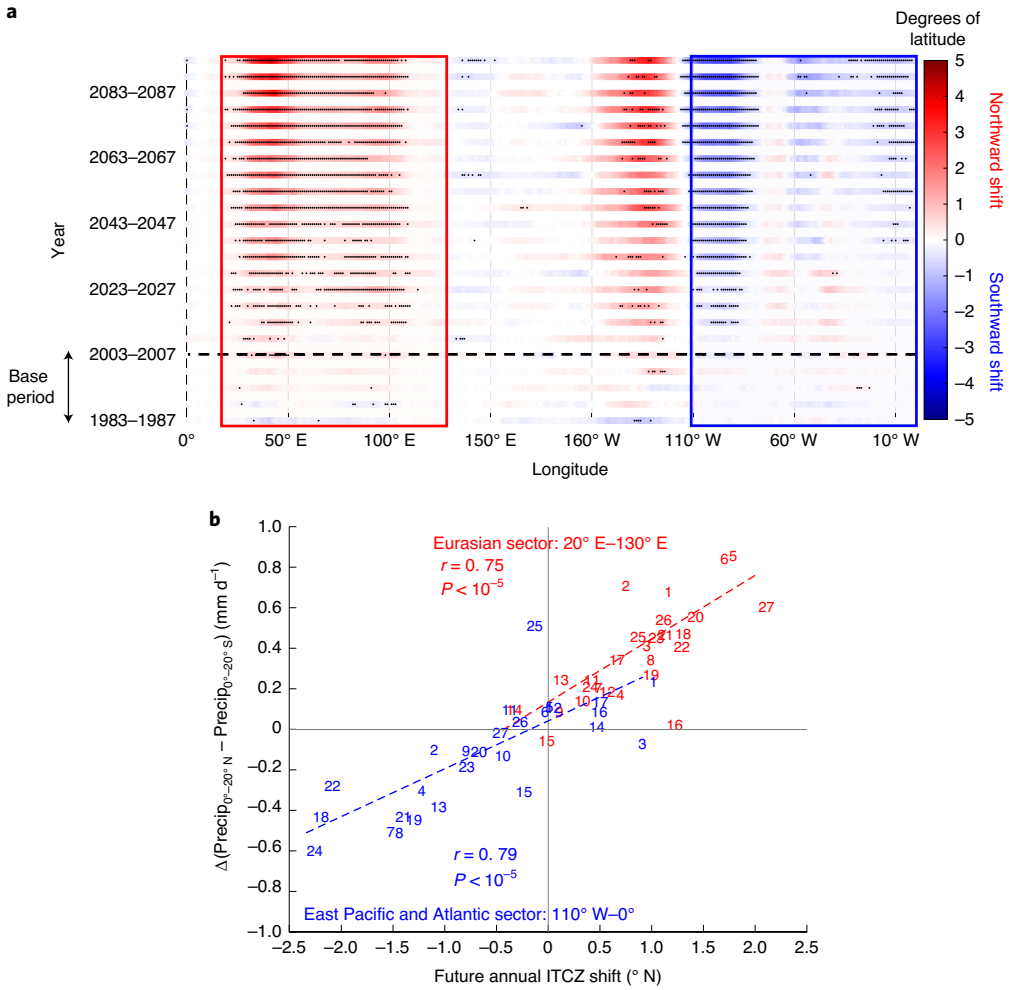

Fig. 2 | Twenty-first-century series of ITCZ location as projected by CMIP6 models. a, Series of the 5-yr-mean ITCZ location relative to the base period as a function of longitude (positive values imply a northward shift). The multimodel mean across 27 CMIP6 models is presented for the SSP3-7.0 scenario; stippling indicates agreement (in the sign of the change) in more than three-fourths of the models considered. **b**, Scatter plot of the projected annual ITCZ shift (horizontal axis) and change of tropical precipitation asymmetry (vertical axis) between the periods 2075–2100 and 1983–2005 using all 27 CMIP6 models zonally averaged over the Eurasian sector (20° E–130° E; red colour) and the eastern Pacific–Atlantic sector (110° W–0°; blue colour). Each model is labelled according to Supplementary Table 1. For models with multiple runs, the average shift across all runs is presented. On the basis of either index (ITCZ shift or precipitation asymmetry), a robust contrasting ITCZ response between the two sectors is visible, whereby the ITCZ is projected to shift northward in the Eurasian sector and southward in the eastern Pacific–Atlantic sector. The northward ITCZ shift shown in panel **a** over 160° W–110° W is an artifact coming from the negative pattern at 25° S shown in Fig. 1c, which dominates the change of the mean of the PDF in these longitudes.

response of the ITCZ, more insight is needed as to why these SST changes occur. Both local and non-local process chains are relevant. For example, the positive IOD pattern in the Indian Ocean has been argued to be a result of the weakening of the Walker circulation locally, but also influenced at its southern margin by the oceanic lateral advection of relatively weak warming signatures from the remote Southern Ocean (Fig. 3a)[47,64–66]. Other non-local mechanisms include extratropics-to-tropics teleconnections, which are usually based on energetic arguments[47,67]. Indeed, in the past two decades, many studies have utilized atmospheric energetic constraints to gain insight into past or future zonal-mean ITCZ shifts[1,5,6,9,12,16,25,67–75]. More recently, similar arguments have been developed[10,76] and used to explain longitudinally varying ITCZ shifts[76–79]. Here we examine how the zonally contrasting shifts of the ITCZ for the SSP3-7.0 scenario are related to energetic constraints, considering changes in the horizontal AET and sector-mean shifts of the EFE.

In response to climate change, models indicate that the net energy input into the atmosphere (schematic in Fig. 4a) will increase in the tropics and decrease at high latitudes 50°–70°, especially over the ocean (see Fig. 4b–d for the change in the total energy input and its partitioning into top-of-atmosphere (TOA) and surface components[80]). In particular, over the Atlantic Ocean, a pattern of northern atmospheric cooling and southern heating is revealed, which is consistent with a future weakening in the AMOC (the see-saw response)[22,34,35,37,81–83], while over the Southern Ocean, atmospheric cooling is consistent with increased heat flux from the atmosphere to the ocean (ocean heat uptake[64–66]) in response to increasing emissions of greenhouse gases[84]. Moreover, we find an increase in atmospheric heating over the tropics, which is mostly a result of the TOA component of the budget (Fig. 4c) and is probably associated with increasing water vapour and anthropogenic greenhouse gases and cloud radiative effects; that is, the OLR escaping to space is reduced in the future (see partitioning of TOA energy change in Supplementary Fig. 9c and ref. [22]). Over land, the effect of decreasing snow and ice albedo (see Supplementary Fig. 9b and studies regarding climate change-induced glacier melting over the Himalayas[29,30] and climate

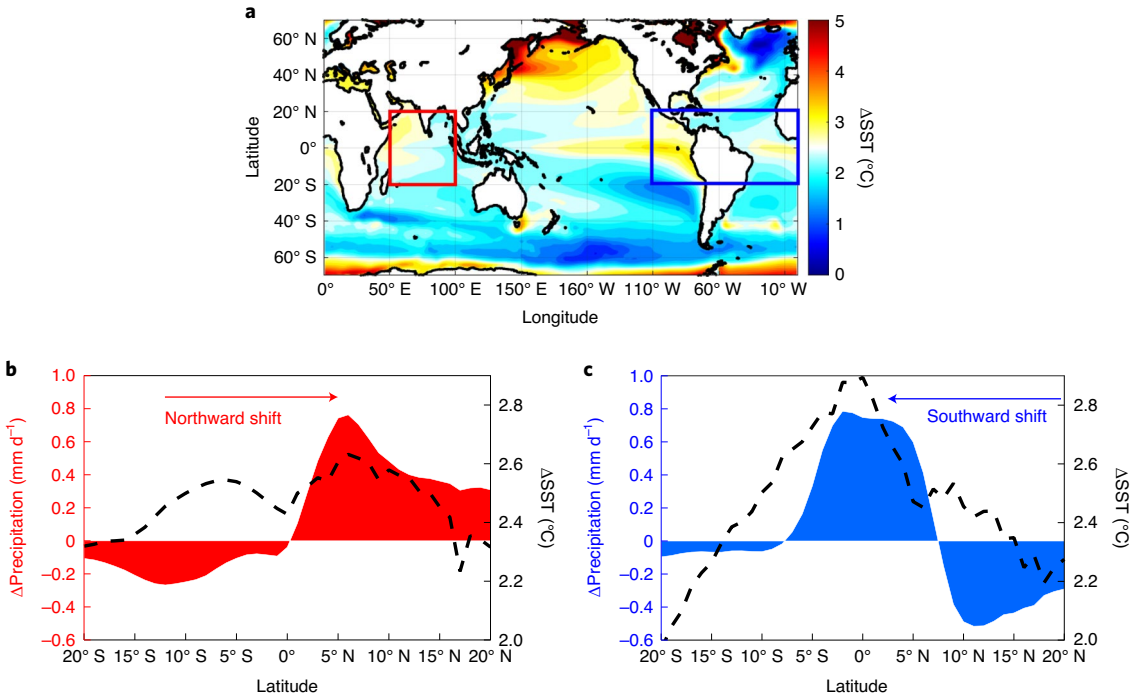

Fig. 3 | Future changes in SST and precipitation in response to climate change, as projected by CMIP6 models. a, Global changes in SST between future (2075–2100) and base (1983–2005) periods. Red and blue boxes correspond to the geographical areas analysed in panels **b** and **c**, respectively. **b**, Zonal mean over the Indian Ocean (50° E–100° E) of the changes of precipitation (mm d^{-1}) and SST (°C) between future (2075–2100) and base (1983–2005) periods. **c**, Same as in **b**, but for the eastern Pacific and Atlantic oceans (110° W–0°); land changes are not considered in the zonal mean. All results refer to the multimodel mean across 27 CMIP6 models for the SSP3-7.0 scenario.

change-induced sea-ice loss in the Arctic[27,31,85]) and reduction of anthropogenic aerosols[22,26] are partially compensated by increases in OLR cooling (Supplementary Fig. 9c). We find that the net effect of all these processes leads to more energy being added into the atmosphere over land in the Northern Hemisphere and specifically over Europe, Southeast Asia, North America and the Arctic (Fig. 4b).

In terms of the zonal mean, the net effect of all these processes leads to an almost zero change in the inter-hemispheric energy asymmetry. In particular, CMIP6 models predict a change on the order of $\Delta(Q_S - Q_N) = -0.05 \pm 0.21$ PW (Q_S and Q_N refer to the hemisperically integrated atmospheric energy input over the Southern and Northern hemispheres, respectively) and consistent with the negligible zonal-mean ITCZ shift reported in Table 1. However, when considering the Eurasian sector and the eastern Pacific–Atlantic sector separately, models show a high level of consensus in terms of the sign of the change over each sector (changes are assessed statistically significant; $P < 0.01$). Over the Eurasian sector, most models predict that more energy is added into the Northern Hemisphere than into the Southern Hemisphere in response to climate change (Fig. 4e), which reduces the baseline inter-hemispheric energy asymmetry; that is, $\Delta(Q_S - Q_N) = -0.24 \pm 0.10$ PW (Table 1). By contrast, over the eastern Pacific–Atlantic sector, the Northern Hemisphere atmosphere receives less energy in the future (Fig. 4e), probably due to the weakening of the AMOC, which contributes to a Northern Hemisphere atmospheric cooling; that is, $\Delta(Q_S - Q_N) = 0.31 \pm 0.16$ PW.

The preceding results highlight contrasting changes of the inter-hemispheric energy asymmetry to climate change between the two considered sectors. To elucidate how these changes alter the AET in the tropics and, thus, the ITCZ, we used a regional energetics framework (Methods)[10,76], which has only recently been applied to explain sector-mean ITCZ shifts[10,76–79], and to the best of our knowledge, it has not yet been applied to scenarios of future climate change.

Our results show that a robust increase of southward AET occurs over the tropics in the Eurasian sector (Fig. 5a; baseline results for the AET are shown in Supplementary Fig. 10), which is consistent with the revealed northward shift of the ITCZ. By contrast, the future cooling over the northern Atlantic Ocean is compensated by changes in the extratropical divergent AET (probably controlled by extratropical eddies; Fig. 4b) but also by a robust increase in the northward energy transport over the tropics of the eastern Pacific–Atlantic sector (Fig. 5a), which is consistent with the revealed southward shift of the ITCZ in this sector. Similarly to the changes in the ITCZ location and in the atmospheric energy input, these results highlight zonally contrasting changes in the meridional component of the divergent AET, providing more confidence regarding the contrasting ITCZ shifts over these two sectors (future changes in zonal energy fluxes are also consistent with the expected weakening of the Walker circulation[47,51]; compare Fig. 5b with Supplementary Fig. 10e).

As a final consistency check of the zonally contrasting ITCZ shifts with regional energetics, we evaluate the future shifts of the EFE (a zone where the AET diverges and vanishes[10]) over the two sectors (Table 1 and Fig. 5c–f). Note that the EFE variability has been shown to be linked with the ITCZ variability, not only in the zonal mean[1,9] but also over large longitudinal sectors, with the ITCZ–EFE link breaking down only over the western and central Pacific[10,86]. Our results show that although CMIP6 models do not predict a robust future EFE shift in the global zonal mean (Table 1), over the Eurasian sector, the EFE shifts to the north by $0.6 \pm 0.4°$, while over the eastern Pacific–Atlantic sector, the EFE shifts to the south by $1.3 \pm 1.2°$ (Fig. 5c). Both these shifts are statistically significant ($P < 0.01$), and they explain around 40% of the intermodel

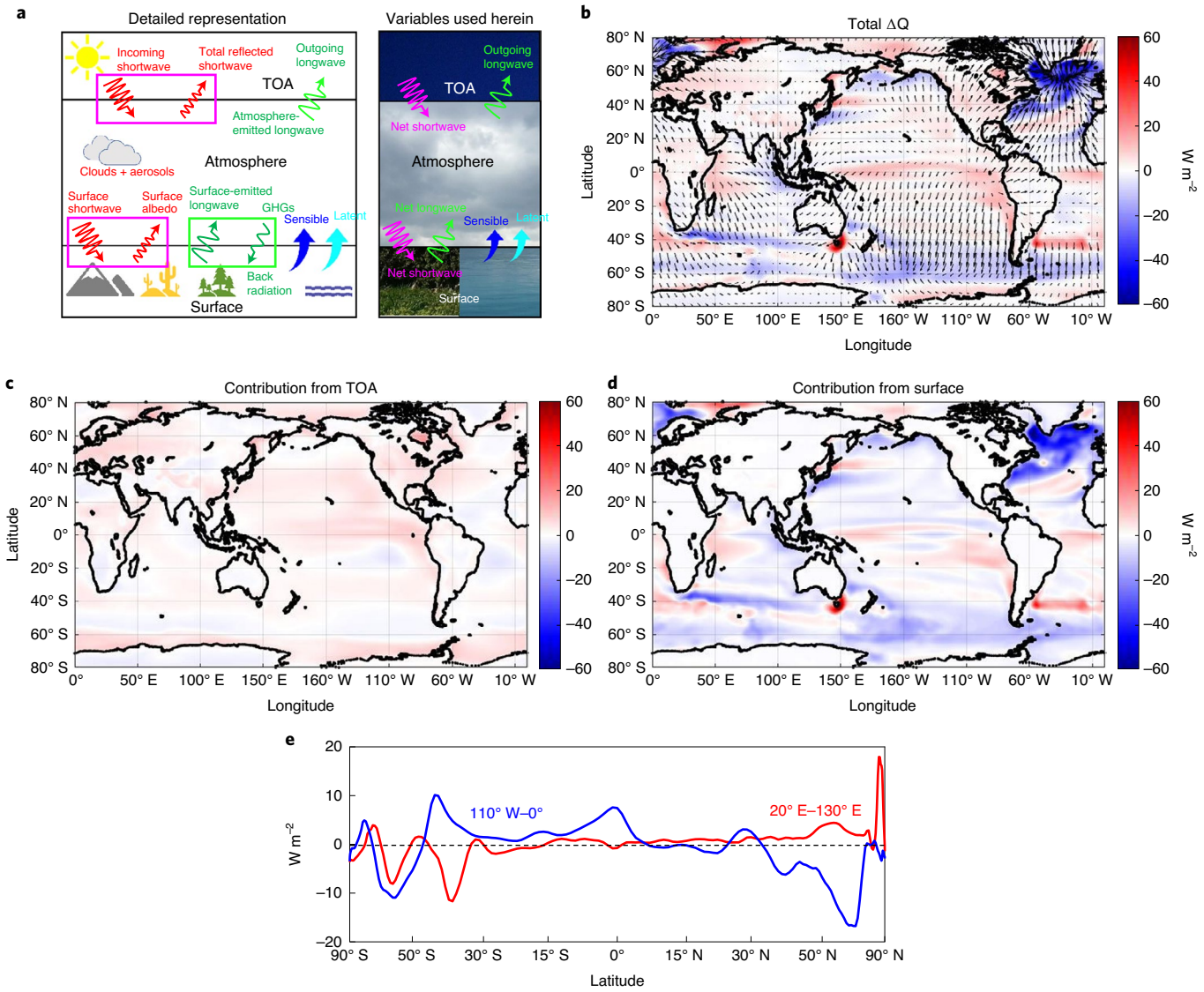

Fig. 4 | Future changes in the atmospheric energy input in response to climate change, as projected by CMIP6 models. a, Graphic representation of the atmospheric energy budget. **b**, Difference of the average net atmospheric energy input between periods 2075–2100 and 1983–2005 (shading). Vectors show the change in the divergent AET; vectors are on the order of 10^7 W m^{-1} (see Fig. 5 for specific values). **c**, Same as in **b**, but only the TOA component is shown. **d**, Same as in **b**, but only the surface component is shown. This panel highlights the contribution of the ocean to the future atmospheric heating/cooling. **e**, Zonal mean of the future change in the net atmospheric energy input (shading in **b**) over the Eurasian sector (20° E–130° E; red curve) and the eastern Pacific–Atlantic sector (110° W–0°; blue curve). The horizontal axis is scaled as sin(φ) (ref. [72]). In all plots, the multimodel mean across 27 CMIP6 models is presented for the SSP3-7.0 scenario. Results show that under global climate change, more energy is added in the atmosphere over the Northern Hemisphere than over the Southern Hemisphere in the Eurasian sector, while the opposite is true in the eastern Pacific–Atlantic sector.

variance of the projected precipitation change (Fig. 5d). Similar EFE shifts are obtained when using an analytic approximation (Methods and ref. [10]) to calculate the EFE latitude (Table 1, Fig. 5e and Supplementary Fig. 11). On the basis of this approximation, we find that future EFE shifts are driven mostly by changes in the cross-equatorial AET and less by changes in the net energy input at the Equator (Fig. 5f).

Overall, our results show that the zonal differences in the ITCZ response to climate change have a robust statistical and physical link with sector-mean changes in the atmosphere's energy budget. It can also be concluded that CMIP6 models do exhibit consensus over the two considered sectors, highlighting contrasting ITCZ shifts, contrasting changes in the atmospheric energy input and contrasting EFE shifts. The longitudinally varying response of all these quantities and the corresponding models' consensus have been hidden in the zonal-mean analysis of past work. We have repeated the analysis using 31 CMIP5 models forced with the RCP 8.5 scenario, which yield similar conclusions (Supplementary Fig. 12 and Supplementary Table 2), although the precipitation shift over the Atlantic is less robust, probably due to higher double-ITCZ biases and intermodel spread in CMIP5[87].

Discussion

In this study, the future shifts of the ITCZ in response to climate change were explored as a function of longitude and season using climate model simulations from CMIP6. We find a zonally contrasting response of the location of the ITCZ, which is robust across different climate models and different seasons. The sector-wide differences in the ITCZ response are spatially extensive, covering about two-thirds of the globe. The contrasting ITCZ response can

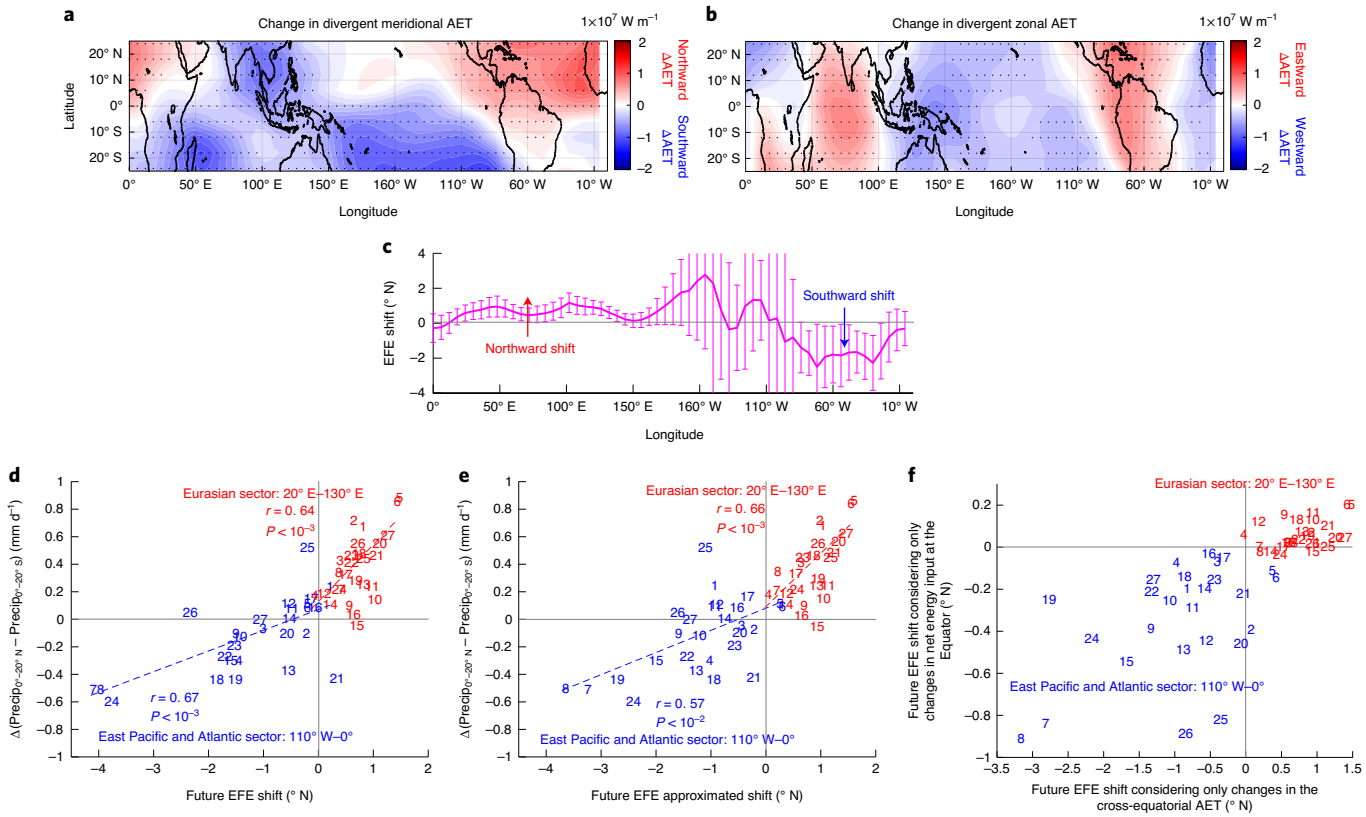

Fig. 5 | Future changes in the AET over the tropics and the EFE in response to climate change, as projected by CMIP6 models. a, Change in the divergent meridional component of the AET over the tropics between periods 2075–2100 and 1983–2005. The multimodel mean across 27 CMIP6 models is presented for the SSP3-7.0 scenario; stippling indicates agreement (in the sign of the change) in more than three-fourths of the models considered. **b**, Same as in **a**, but for the divergent zonal component. **c**, Future EFE shift as a function of longitude between periods 2075–2100 and 1983–2005. EFE is tracked by the latitude where the divergent meridional AET diverges and vanishes. The magenta curve shows the multimodel mean, while the error bars show the intermodel spread (±s.d.). **d**, Change in the precipitation asymmetry (between periods 2075–2100 and 1983–2005) as a function of the EFE shift, using all 27 CMIP6 models zonally averaged over the Eurasian sector (20° E–130° E; red colour) and the eastern Pacific–Atlantic sector (110° W–0°; blue colour). Each model is labelled according to Supplementary Table 1. For models with multiple runs, the average shift across all runs is presented. **e**, Same as in **d**, but the EFE shifts are approximated using the analytic expression in Equation (4) (Methods). **f**, The EFE shifts in **e** are decomposed into shifts that consider changes only in the cross-equatorial AET (horizontal axis) or only in net energy input at the Equator (vertical axis). Results show that with climate change, the future state of the AET will be characterized by an increased southward transport (divergent component) over the tropical Eurasian sector, which implies a northward shift of EFE, and it is statistically consistent with a northward shift of the ITCZ. The opposite (increased northward energy transport and southward shift of EFE) is true in the eastern Pacific–Atlantic sector. In addition, future EFE shifts are shown to be dominated by changes in the cross-equatorial AET.

be summarized as a northward shift over eastern Africa and the Indian Ocean and a southward shift over the eastern Pacific Ocean, South America and the Atlantic Ocean. The longitudinally varying ITCZ response and its robustness have often been masked in previous analyses focusing on zonal-mean ITCZ shifts.

We find that the contrasting ITCZ response is driven by a positive IOD-like SST pattern over the Indian Ocean, and high SST warming near the Equator over the eastern Pacific and Atlantic oceans that serves as an attractor for a southward shift of the ITCZ from its current position. From an atmospheric energetics perspective, our analysis shows that future climate change induces a zonally contrasting change in the inter-hemispheric heating of the atmosphere as a result of the combined effect of radiative and dynamical processes in both the atmosphere and the ocean. Most models show that future changes consist of increases in atmospheric heating over Eurasia and cooling over the Southern Ocean, which contrasts with atmospheric cooling over the North Atlantic Ocean as a consequence of a projected AMOC weakening[34,35]. These changes in the regional extratropical atmospheric heating induce an increase in the southward energy transport over the tropics of eastern Africa and the Indian Ocean (and a northward shift of the EFE) and an increase in the northward energy transport over the tropical eastern Pacific–Atlantic sector (and a southward shift of the EFE), both of which are physically and statistically consistent with the revealed ITCZ response. Our results provide a single theoretical framework for simultaneously explaining anticipated future increases of drought stress in southeastern Africa and Madagascar, intensifying flooding in southern India[56] and greater drought stress in Central America[38]—large hydrological hotspots of global change[88,89] that will have considerable impacts on food security and biodiversity.

We note that although our study establishes consistency between the energetics framework and projected changes in tropical precipitation, only about 40% of the intermodel variance of precipitation change is explained on the basis of energetic arguments. This highlights the important limitations of the energetics framework, already reported in the literature (not only in regional settings[90] but also in the zonal mean[46,91,92]), and the need to further explore mechanisms involving ocean–atmosphere–land coupling at regional scales. To further infer causality, carefully designed idealized climate experiments are needed as a complement to analyses like this one that

attempt to understand mechanisms contributing to robust future changes in the hydrological cycle within and across different Earth system models.

Online content

Any methods, additional references, Nature Research reporting summaries, source data, extended data, supplementary information, acknowledgements, peer review information; details of author contributions and competing interests; and statements of data and code availability are available at https://doi.org/10.1038/s41558-020-00963-x.

Received: 2 September 2019; Accepted: 9 November 2020;
Published online: 18 January 2021

References

1. Schneider, T., Bischoff, T. & Haug, G. H. Migrations and dynamics of the intertopical convergence zone. *Nature* https://doi.org/10/nature13636 (2014).
2. Waliser, D. E. & Gautier, C. A satellite-derived climatology of the ITCZ. *J. Clim.* **6**, 2162–2174 (1993).
3. Trenberth, K. E., Stepaniak, D. P. & Caron, J. M. The global monsoon as seen through the divergent atmospheric circulation. *J. Clim.* **13**, 3969–3993 (2000).
4. Adler, R. F. et al. The Version-2 global precipitation climatology project (GPCP) monthly precipitation analysis (1979–present). *J. Hydrometeorol.* **4**, 1147–1167 (2003).
5. Donohoe, A., Marshall, J., Ferreira, D. & McGee, D. The relationship between ITCZ location and cross-equatorial atmospheric heat transport: from the seasonal cycle to the last glacial maximum. *J. Clim.* https://doi.org/10.1175/JCLI-D-12-00467.1 (2013).
6. Bischoff, T. & Schneider, T. Energetic constraints on the position of the intertropical convergence zone, *J. Clim.* https://doi.org/10.1175/JCLI-D-13-00650.1 (2014).
7. Berry, G. & Reeder, M. J. Objective identification of the intertropical convergence zone: climatology and trends from the ERA-interim. *J. Clim.* **27**, 1894–1909 (2014).
8. Wang, C. & Magnusdottir, G. The ITCZ in the central and eastern Pacific on synoptic time scales. *Mon. Weather Rev.* **134**, 1405–1421 (2006).
9. Adam, O., Bischoff, T. & Schneider, T. Seasonal and interannual variations of the energy flux equator and ITCZ. Part I: zonally averaged ITCZ position. *J. Clim.* **29**, 3219–3230 (2016).
10. Adam, O., Bischoff, T. & Schneider, T. Seasonal and interannual variations of the energy flux equator and ITCZ. Part II: zonally varying shifts of the ITCZ. *J. Clim.* **29**, 7281–7293 (2016).
11. Chou, C., Tu, J.-Y. & Tan, P.-H. (2007) Asymmetry of tropical precipitation change under global warming. *Geoph. Res. Lett*. https://doi.org/10.1029/2007GL030327 (2007).
12. Sachs, J. P. et al. Southward movement of the Pacific intertropical convergence zone AD 1400–1850. *Nat. Geosci.* https://doi.org/10.1038/NGEO554 (2009).
13. Cai, W. et al. More extreme swings of the South Pacific convergence zone due to greenhouse warming. *Nature* **488**, 365–369 (2012).
14. Broecker, W. S. & Putnam, A. E. Hydrologic impacts of past shifts of Earth's thermal equator offer insight into those to be produced by fossil fuel CO_2. *Proc. Natl Acad. Sci. USA* **110**, 16710–16715 (2013).
15. Arbuszewski, J. A., De Menocal, P. B., Cléroux, C., Bradtmiller, L. & Mix, A. Meridional shifts of the Atlantic intertropical convergence zone since the Last Glacial Maximum. *Nat. Geosci.* https://doi.org/10.1038/NGEO1961 (2013).
16. Hwang, Y.-T., Frierson, D. M. W. & Kang, S. M. Anthropogenic sulfate aerosol and the southward shift of tropical precipitation in the late 20th century, *Geoph. Res. Lett*. https://doi.org/10.1002/grl.50502 (2013).
17. Lau, W. K. M. & Kim, K.-M. Robust Hadley circulation changes and increasing global dryness due to CO_2 warming from CMIP5 model projections. *Proc. Natl Acad. Sci. USA* **112**, 3630–3635 (2015).
18. Allen, R. J. A 21st century northward tropical precipitation shift caused by future anthropogenic aerosol reductions. *J. Geophys. Res. Atmos.* **120**, 9087–9102 (2015).
19. Allen, R. J., Evan, A. T. & Booth, B. B. B. Interhemispheric aerosol radiative forcing and tropical precipitation shifts during the late twentieth century. *J. Clim.* https://doi.org/10.1175/JCLI-D-15-0148.1 (2015).
20. Byrne, M. P. & Schneider, T. Narrowing of the ITCZ in a warming climate: physical mechanisms. *Geophys. Res. Lett.* **43**, 11350–11357 (2016).
21. Chung, E.-S. & Soden, B. J. Hemispheric climate shifts driven by anthropogenic aerosol–cloud interactions. *Nat. Geosci.* https://doi.org/10.1038/NGEO2988 (2017).
22. McFarlane, A. A. & Frierson, D. M. W. The role of ocean fluxes and radiative forcings in determining tropical rainfall shifts in RCP 8.5 simulations. *Geophys. Res. Lett.* **44**, 8656–8664 (2017).
23. Bony, S. et al. Clouds, circulation and climate sensitivity. *Nat. Geosci.* **8**, 261–268 (2015).
24. Cox, P. M. et al. Increasing risk of Amazonian drought due to decreasing aerosol pollution. *Nature* **453**, 212–215 (2008).
25. Rotstayn, L., Collier, M. & Luo, J. Effects of declining aerosols on projections of zonally averaged tropical precipitation. *Environ. Res.* **10**, 044018 (2015).
26. Lamarque, J. M. et al. Global and regional evolution of shortlived radiatively-active gases and aerosols in the representative concentration pathways. *Climatic Change* **109**, 191–212 (2011).
27. Serreze, M. C. & Barry, R. G. Processes and impacts of Arctic amplification: a research synthesis. *Glob. Planet. Change* **77**, 85–96 (2011).
28. Labe, Z., Magnusdottir, G. & Stern, H. Variability of Arctic sea ice thickness using PIOMAS and the CESM large ensemble. *J. Clim.* **31**, 3233–3247 (2018).
29. Immerzeel, W. W., Pellicciotti, F. & Bierkens, M. F. P. Rising river flows throughout the twenty-first century in two Himalayan glacierized watersheds. *Nat. Geosci.* **6**, 742–745 (2013).
30. Chaturvedi, R. K., Kulkarni, A., Karyakarte, Y., Joshi, J. & Bala, G. Glacial mass balance changes in the Karakoram and Himalaya based on CMIP5 multi-model climate projections. *Climatic Change* **123**, 315–328 (2014).
31. Tomas, R. A., Deser, C. & Sun, L. The role of ocean heat transport in the global climate response to projected Arctic sea ice loss. *J. Clim.* **29**, 6841–6859 (2016).
32. Weaver, A. J. et al. Stability of the Atlantic meridional overturning circulation: a model intercomparison. *Geophys. Res. Lett.* **39**, L20709 (2012).
33. Cheng, W., Chiang, J. C. H. & Zhang, D. Atlantic meridional overturning circulation (AMOC) in CMIP5 models: RCP and historical simulations. *J. Clim.* **26**, 7187–7197 (2013).
34. Rahmstorf, S. et al. Exceptional twentieth-century slowdown in Atlantic Ocean overturning circulation. *Nat. Clim. Change* **5**, 475–480 (2015).
35. Weijer, W., Cheng, W., Garuba, O. A., Hu, A. & Nadiga, B. T. (2020) CMIP6 models predict significant 21st century decline of the Atlantic meridional overturning circulation. *Geophys. Res. Lett*. https://doi.org/10.1029/2019GL086075 (2020).
36. Caesar, L., Rahmstorf, S., Robinson, A., Feulner, G. & Saba, V. Observed fingerprint of a weakening Atlantic Ocean overturning circulation. *Nature* **556**, 191–196 (2018).
37. Zhang, R. & Delworth, T. L. Simulated topical response to a substantial weakening of the Atlantic thermohaline circulation. *J. Clim.* **18**, 1853–1860 (2005).
38. Chen, Y., Langenbrunner, B. & Randerson, J. T. Future drying in Central America and northern South America linked with Atlantic meridional overturning circulation. *Geophys. Res. Lett.* **45**, 9226–9235 (2018).
39. Eyring et al. An overview of the Coupled Model Intercomparison Project phase 6 (CMIP6) experimental design and organization. *Geosci. Model Dev.* **9**, 1937–1958 (2016).
40. O'Neill, B. C. et al. The roads ahead: narratives for shared socioeconomic pathways describing world futures in the 21st century. *Glob. Environ. Change* **42**, 169–180 (2017).
41. Van Vuuren, D. P. et al. Representative concentration pathways: an overview. *Climatic Change* **109**, 5–31 (2011).
42. Nicholson, S. E. The ITCZ and the seasonal cycle over equatorial Africa. *Bull. Am. Meteorol. Soc.* **99**, 337–348 (2018).
43. Mamalakis, A. & Foufoula-Georgiou, E. A multivariate probabilistic framework for tracking the intertropical convergence zone: analysis of recent climatology and past trends. *Geophys. Res. Lett*. https://doi.org/10.1029/2018GL079865 (2018).
44. Byrne, M. P., Pendergrass, A. G., Rapp, A. D. & Wodzicki, K. R. Response of the intertropical convergence zone to climate change: location, width, and strength. *Curr. Clim. Change Rep.* **4**, 355–370 (2018).
45. Pauluis, O. Boundary layer dynamics and cross-equatorial Hadley circulation. *J. Atmos. Sci.* **61**, 1161–1173 (2004).
46. Wei, H.-H. & Bordoni, S. Energetic constraints on the ITCZ position in idealized simulations with a seasonal cycle. *J. Adv. Model. Earth Syst.* **10**, 1708–1725 (2018).
47. Xie, S.-P. et al. Global warming pattern formation: sea surface temperature and rainfall. *J. Clim.* **23**, 966–986 (2010).
48. Dutheil, C. et al. Impact of temperature biases on climate change projections of the South Pacific Convergence Zone. *Clim. Dyn*. https://doi.org/10.1007/s00382-019-04692-6 (2019).
49. Kang, S. M. & Held, I. M. Tropical precipitation, SSTs and the surface energy budget: a zonally symmetric perspective. *Clim. Dyn.* **38**, 1917–1924 (2012).
50. Xiang, B., Zhao, M., Ming, Y., Yu, W. & Kang, S. M. Contrasting impacts of radiative forcing in the Southern Ocean versus southern tropics on ITCZ position and energy transport in one GFDL climate model. *J. Clim.* **31**, 5609–5628 (2018).
51. Vecchi, G. A. & Soden, B. J. Global warming and the weakening of the tropical circulation. *J. Clim.* **20**, 4316–4340 (2007).
52. Saji, N. H., Goswami, B. N., Vinayachandran, P. N. & Yamagata, T. A dipole mode in the tropical Indian Ocean. *Nature* **401**, 360–363 (1999).

53. Seth, A. et al. Enhanced spring convective barrier for monsoons in a warmer world? *Climatic Change* **104**, 403–414 (2011).
54. Seth, A. et al. CMIP5 projected changes in the annual cycle of precipitation in monsoon regions. *J. Clim.* **26**, 7328–7351 (2013).
55. Rodríguez-Fonseca, B. et al. Variability and predictability of West African droughts: a review on the role of sea surface temperature anomalies. *J. Clim.* **28**, 4034–4060 (2015).
56. D'Agostino, R., Bader, J., Bordoni, S., Ferreira, D. & Jungclaus, J. Northern Hemisphere monsoon response to mid-Holocene orbital forcing and greenhouse gas-induced global warming. *Geophys. Res. Lett.* **46**, 1591–1601 (2019).
57. Pascale, S., Carvalho, L. M. V., Adams, D. K., Castro, C. L. & Cavalcanti, I. F. A. Current and future variations of the monsoons of the Americas in a warming climate. *Curr. Clim. Change Rep.* **5**, 125–144 (2019).
58. Zilli, M. T., Carvalho, L. M. V. & Lintner, B. R. The poleward shift of South Atlantic convergence zone in recent decades. *Clim. Dyn.* **52**, 2545–2563 (2019).
59. Dunning, C. M., Black, E. & Allan, R. P. Later wet seasons with more intense rainfall over Africa under future climate change. *J. Clim.* **31**, 9719–9738 (2018).
60. Cook, K. H. & Vizy, E. K. Impact of climate change on mid-twenty-first century growing seasons in Africa. *Clim. Dyn.* **39**, 2937–2955 (2012).
61. Menon, A., Levermann, A., Schewe, J., Lehmann, J. & Frieler, K. Consistent increase in Indian monsoon rainfall and its variability across CMIP-5 models. *Earth. Sys. Dyn.* **4**, 287–300 (2013).
62. Sharmila, S., Joseph, S., Sahai, A. K., Abhilash, S. & Chattopadhyay, R. Future projection of Indian summer monsoon variability under climate change scenario: an assessment from CMIP5 climate models. *Glob. Planet. Change* **124**, 62–78 (2015).
63. Kooperman, G. J. et al. Forest response to rising CO_2 drives zonally asymmetric rainfall change over tropical land. *Nat. Clim. Change* **8**, 434–440 (2018).
64. Hwang, Y.-T., Xie, S.-P., Deser, C. & Kang, S. M. Connecting tropical climate change with Southern Ocean heat uptake. *Geophys. Res. Lett.* **44**, 9449–9457 (2017).
65. Frölicher, T. L. et al. Dominance of the Southern Ocean in anthropogenic carbon and heat uptake in CMIP5 models. *J. Clim.* **28**, 862–886 (2015).
66. Roemmich, D. et al. Unabated planetary warming and its ocean structure since 2006. *Nat. Clim. Change* **5**, 240–254 (2015).
67. Kang, S. M., Held, I. M., Frierson, D. M. W. & Zhao, M. The response of the ITCZ to extratropical thermal forcing: idealized slab–ocean experiments with a GCM. *J. Clim.* **21**, 3521–3532 (2008).
68. Moreno-Chamarro, E., Marshall, J. & Delworth, T. L. Linking ITCZ migrations to the AMOC and North Atlantic/Pacific SST decadal variability. *J. Clim.* **33**, 893–905 (2020).
69. Haywood, J. M., Jones, A., Bellouin, N. & Stephenson, D. Asymmetric forcing from stratospheric aerosols impacts Sahelian rainfall. *Nat. Clim. Change* **3**, 660–665 (2013).
70. Chiang, J. C. H. & Bitz, C. M. Influence of high latitude ice cover on the marine intertropical convergence zone. *Clim. Dyn.* **25**, 477–496 (2005).
71. Broccoli, A. J., Dahl, K. A. & Stouffer, R. J. Response of the ITCZ to Northern Hemisphere cooling. *Geophys. Res. Lett.* **33**, L01702 (2006).
72. Frierson, D. M. W. & Hwang, Y.-T. Extratropical influence on ITCZ shifts in slab ocean simulations of global warming. *J. Clim.* **25**, 720–733 (2012).
73. Hwang, Y. & Frierson, D. Link between the double-intertropical convergence zone problem and cloud biases over the Southern Ocean. *Proc. Natl Acad. Sci. USA* **110**, 4935–4940 (2013).
74. Green, B. & Marshall, J. Coupling of trade winds with ocean circulation damps ITCZ shifts. *J. Clim.* **30**, 4395–4411 (2017).
75. Yu, S. & Pritchard, M. S. A strong role for the AMOC in partitioning global energy transport and shifting ITCZ position in response to latitudinally discrete solar forcing in the CESM1.2. *J. Clim.* https://doi.org/10.1175/JCLI-D-18-0360.1 (2019).
76. Boos, W. R. & Korty, R. L. Regional energy budget control of the intertropical convergence zone and application to mid-Holocene rainfall. *Nat. Geosci.* **9**, 892–897 (2016).
77. Adam, O., Schneider, T. & Brient, F. Regional and seasonal variations of the double-ITCZ bias in CMIP 5 models. *Clim. Dyn.* https://doi.org/10.1007/s00382-017-3909-1 (2018).
78. Adam, O., Schneider, T., Enzel, Y. & Quade, J. Both differential and equatorial heating contributed to African monsoon variations during mid-Holocene. *Earth Planet. Sci. Lett.* **522**, 20–29 (2019).
79. Lintner, B. & Boos, W. Using atmospheric energy transport to quantitatively constrain South Pacific convergence zone shifts during ENSO. *J. Clim.* **32**, 1839–1855 (2019).
80. Feldl, N. & Bordoni, S. Characterizing the Hadley circulation through regional climate feedbacks. *J. Clim.* **29**, 613–622 (2016).
81. Rahmstorf, S. Ocean circulation and climate during the past 120,000 years. *Nature* **419**, 207–214 (2002).
82. Cheng, W., Bitz, C. M. & Chiang, J. C. H. in *Ocean Circulation: Mechanisms and Impacts* (eds Schmittner, A. et al.) 295–314 (AGU, 2007).
83. Drijfhout, S., van Oldenborgh, G. J. & Cimatoribus, A. Is a decline of AMOC causing the warming hole above the North Atlantic in observed and modeled warming patterns? *J. Clim.* **25**, 8373–8379 (2012).
84. Swart, N. C., Gille, S. T., Fyfe, J. C. & Gillet, N. P. Recent Southern Ocean warming and freshening driven by greenhouse gas emissions and ozone depletion. *Nat. Geosci.* **11**, 836–841 (2018).
85. Deser, C., Tomas, R. A. & Sun, L. The role of ocean–atmosphere coupling in the zonal-mean atmospheric response to Arctic Sea ice loss. *J. Clim.* **28**, 2168–2186 (2015).
86. Wei, H.-H. & Bordoni, S. Energetic constraints on the intertropical convergence zone position in the observed seasonal cycle from Modern-Era Retrospective Analysis for Research and Applications, Version 2 (MERRA-2). *Geophys. Res. Lett.* **47**, e2020GL088506 (2020).
87. Tian, B. & Dong, X. The double-ITCZ bias in CMIP3, CMIP5 and CMIP6 models based on annual mean precipitation. *Geophys. Res. Lett.* **47**, e2020GL087232 (2020).
88. Diffenbaugh, N. S. & Giorgi, F. Climate change hotspots in the CMIP5 global climate model ensemble. *Climatic Change* **114**, 813–822 (2012).
89. Xu, L., Wang, A., Wang, D. & Wang, H. Hot spots of climate extremes in the future. *J. Geophys. Res. Atmos.* **124**, 3035–3049 (2019).
90. Hill, S. A. Theories for past and future monsoon rainfall changes. *Curr. Clim. Change Rep.* **5**, 160–171 (2019).
91. Kang, S. M., Shin, Y. & Xie, S. Extratropical forcing and tropical rainfall distribution: energetics framework and ocean Ekman advection. *NPJ Clim. Atmos. Sci.* **1**, 20172 (2018).
92. Biasutti, M. & Voigt, A. Seasonal and CO_2-induced shifts of the ITCZ: testing energetic controls in idealized simulations with comprehensive models. *J. Clim.* **33**, 2853–2870 (2020).

Publisher's note Springer Nature remains neutral with regard to jurisdictional claims in published maps and institutional affiliations.

© The Author(s), under exclusive licence to Springer Nature Limited 2021

Methods

Probabilistic tracking of the ITCZ. With regard to regionally tracking the ITCZ, ambiguity exists in the literature as to a precise regional definition of the ITCZ and/or which is the optimal variable/method to use for tracking its position[42]. For example, past studies have variously used surface pressure minimum, surface wind convergence, precipitation maximum, minimum OLR or cloudiness maximum to track the ITCZ[42]. The justification for variously using different variables to track the ITCZ is the assumption that the minima or maxima of these variables collocate with each other (pressure minima roughly collocate with convergence maxima and so on). Yet this assumption may not be true over specific regions or in specific seasons[42], and so, this ambiguity in the regional ITCZ definition is problematic. For the purpose of this study, we have used a multivariate probabilistic framework[43], which tracks the ITCZ over different longitudes and seasons by simultaneously assessing the statistics of multiple variables and thus increasing the robustness of the tracking approach (see refs. [59,93,94] for other similar approaches). In particular, we consider overlapping longitudinal windows and use the window zonal-mean precipitation and OLR (the two most common variables in the ITCZ literature) to track the ITCZ. For each window and season, ITCZ points are defined as those that correspond to the maximum (above a certain threshold) joint probability of non-exceedance of the two window zonal-mean variables (note that in cases where precipitation and OLR extrema collocate, the latter definition falls back to simply tracking the points of the extrema, and results would be identical if we were to use either variable on its own). The end product of the method is to provide the probability of every grid point in the tropics to be part of the ITCZ in a longitudinally explicit manner (Supplementary Figs. 1 and 2). The resulting probability distribution of ITCZ position is used to compare the climatology and interannual variability of the ITCZ between observations and CMIP6 models during a contemporary base period (1983–2005) as well as to assess future ITCZ changes (defined as the difference between the period 2075–2100 and the base period).

More specifically, let X denote the variable (for example, precipitation) used for defining the ITCZ location, and $X_w^{\lambda,t}$ the zonal mean of X within the longitudinal window $[\lambda-w/2, \lambda+w/2]$ of width w and during month/season t. The latitudinal distribution of $X_w^{\lambda,t}$ can be obtained from observations or model outputs. For a specified probability of non-exceedance a (tracking threshold), we define $x_{w,a}^{\lambda,t}$ to be the a^{th} quantile of $X_w^{\lambda,t}$, that is:

$$F\left(x_{w,a}^{\lambda,t}\right) \equiv \Pr\left[X_w^{\lambda,t} \le x_{w,a}^{\lambda,t}\right] = a$$

where F is the cumulative distribution function of $X_w^{\lambda,t}$. We define the random variable $\Phi_{w,a}^{\lambda,t}$ to be the location (in degrees of latitude) at which the ITCZ is most likely to prevail, in longitude λ and in month/season t. A sample of $\Phi_{w,a}^{\lambda,t}$ may then be the set of latitudinal points $\varphi_{w,a}^{\lambda,t}$ at which the value of $X_w^{\lambda,t}$ exceeds the a^{th} quantile $x_{w,a}^{\lambda,t}$, that is:

$$\left\{\varphi_{w,a}^{\lambda,t}\right\} : X_w^{\lambda,t}\left(\varphi_{w,a}^{\lambda,t}\right) > x_{w,a}^{\lambda,t} = F^{-1}(a)$$

or

$$\left\{\varphi_{w,a}^{\lambda,t}\right\} : F\left(X_w^{\lambda,t}\left(\varphi_{w,a}^{\lambda,t}\right)\right) > a \quad (1)$$

In other words, we track the position of ITCZ using the upper $(1-a)\times 100\%$ of precipitation in longitude λ and month/season t, which corresponds to the points $\varphi_{w,a}^{\lambda,t}$. When considering the OLR to track the ITCZ, the negative OLR is used since deep convection associates with minimum (not maximum) OLR. Such an approach is rather computationally efficient and allows the analysis of both the annual-mean location and the intra-annual variability of the ITCZ simply by obtaining the ITCZ points, $\varphi_{w,a}^{\lambda,t}$, for each calendar month or each season.

When jointly considering multiple (for example, $M \ge 2$) variables $\mathbf{X} = [X_1, X_2, \ldots, X_M]$ to track the ITCZ (as in this study), the ITCZ points, $\varphi_{w,a}^{\lambda,t}$, also satisfy Equation (1), but F is now the joint cumulative distribution function of $\mathbf{X}_w^{\lambda,t}$.

Herein, we used a non-exceedance $a = 85\%$ as a tracking threshold (general conclusions have been tested across other thresholds, too, to ensure robustness), and we averaged precipitation and OLR over overlapping longitudinal windows of width $w = 15°$ (see Supplementary Figs. 1 and 2 for schematics). However, the framework is general and applicable in considering any single variable and/or jointly distributed multiple variables to define the ITCZ. See ref. [43] for more information.

Atmospheric energy budget. Considering a long enough period (for example, 1983–2005) so that the energy storage in the atmosphere is negligible[1,95], and assuming that the system is in equilibrium, the atmospheric energy budget is [6,95]:

$$\nabla \cdot \mathbf{F} = R^{\text{TOA}} - O = Q \quad (2)$$

where $\mathbf{F}$ is the vector of vertically integrated atmospheric moist static energy flux, R^{TOA} is the net energy input at the TOA (net downward shortwave minus the outgoing longwave radiation) and O is the ocean energy uptake (can be further partitioned into latent/sensible heat and radiative surface components) and represents the heating from the surface (note that the energy storage in the land is negligible on timescales greater than a season[1]). Q is the net energy input into the atmospheric column of unit horizontal area (see schematic in Fig. 4a and Supplementary Fig. 10a,b for the distribution of Q in the base period), and Equation (2) states that it is equal to the horizontal divergence of the AET.

Regional energetics–EFE latitude approximation. The energy flux $\mathbf{F}$ in Equation (2) can be decomposed into the divergent and rotational components ($\mathbf{F}_\chi$ and $\mathbf{F}_\psi$, respectively), and since the divergence of the rotational component is identically zero ($\nabla\cdot\mathbf{F}_\psi = 0$), Equation (2) takes the form of Poisson's equation:

$$\nabla \cdot \mathbf{F}_\chi = \nabla^2\chi = Q \quad (3)$$

where χ is the energy flux potential (an arbitrary scalar function)[10,76], such that its gradient is equal to the divergent component of AET; that is, $(\partial_x\chi, \partial_y\chi) = \nabla\chi = \mathbf{F}_\chi = (u_\chi, v_\chi)$. By solving Equation (3), the potential χ (also $\mathbf{F}_\chi$) can be obtained; all derivatives are evaluated in spherical coordinates but written here in Cartesian coordinates for simplicity. The zonal component of the divergent AET is negligible relative to the meridional component outside from the tropics ($v_\chi >> u_\chi$; Supplementary Fig. 10c), while in the tropics, they are of the same magnitude (both the Walker and Hadley circulations contribute to the divergence of heat; Supplementary Fig. 10d,e)[10,76,77].

For a sector with longitudinal boundaries λ_1 and λ_2, the sector-mean position of the EFE (or equivalently of the ITCZ) can be approximated to a first order by meridionally expanding (Taylor series) Equation (3) at the Equator[10]:

$$\left[\varphi_{\text{EFE}}\right]_{\lambda_1}^{\lambda_2} = -\frac{1}{a}\frac{\left[v_{\chi_0}\right]_{\lambda_1}^{\lambda_2}}{\left[Q_0\right]_{\lambda_1}^{\lambda_2} - \frac{1}{\lambda_2-\lambda_1}u_{\chi_0}\Big|_{\lambda_1}^{\lambda_2}} \quad (4)$$

where $[.]_{\lambda_1}^{\lambda_2}$ represents the zonal mean over the sector, subscript '0' represents average values near the Equator and a is Earth's radius.

Definition of ITCZ bias in the models. The double-ITCZ bias of each CMIP6 model over the eastern Pacific or Atlantic Ocean is defined as the average (over the considered longitudinal sector) difference in the November–April probability distribution of the ITCZ location between the model and the observations (Supplementary Fig. 6):

$$\Delta P = \frac{1}{\frac{(\lambda_2-\lambda_1)}{r_\lambda}+1}\sum_{\lambda=\lambda_1}^{\lambda_2}\left(\frac{1}{2}\int_{\varphi_1}^{\varphi_2}\left|\Delta\text{PDF}_{\lambda,\varphi}\right|d\varphi\right) \quad (5)$$

where $\Delta\text{PDF}_{\lambda\varphi}$ is the difference in the November–April PDF of the ITCZ location between the model and the observations at latitude φ and longitude λ, and r_λ is the model's longitudinal resolution. For calculating the bias over the Atlantic Ocean, $[\varphi_1, \varphi_2] = [15°\,\text{S}, 10°\,\text{N}]$ and $[\lambda_1, \lambda_2] = [50°\,\text{W}, 0°]$, while for the eastern Pacific bias, $[\varphi_1, \varphi_2] = [10°\,\text{S}, 15°\,\text{N}]$ and $[\lambda_1, \lambda_2] = [160°\,\text{W}, 60°\,\text{W}]$. The ITCZ biases of all models are presented in Supplementary Table 1. The average bias (weighted by the longitudinal width of each sector) is also presented.

Correlation significance. For estimating the $(1-P)$% intervals corresponding to statistically insignificant linear correlation (for a p-value P), we assume a t distribution: $r_c = \frac{\pm t}{\sqrt{N-2+t^2}}$, where t is the $(1-P/2)$% quantile of the t distribution, with d.f. $= N-2$, and N is the sample size.

Data availability

The data we use in our analysis are all freely available. We use satellite data (monthly precipitation series on a $0.25°\times 0.25°$ grid[96] and OLR series on a $1°\times 1°$ grid[97] for 1983–2005) and climate model outputs from the sixth phase of the Coupled Model Intercomparison Project[39] (CMIP6); see Supplementary Table 1.

Code availability

Upon reasonable request, the code that supports the findings of this study can be provided by the corresponding author.

References

93. Shonk, J. K. P. et al. Identifying causes of western Pacific ITCZ drift in ECMWF System 4 hindcasts. *Clim. Dyn.* **50**, 939–954 (2018).
94. Bain, C. L. et al. Detecting the ITCZ in instantaneous satellite data using spatiotemporal statistical modeling: ITCZ climatology in the east Pacific. *J. Clim.* https://doi.org/10.1175/2010JCLI3716.1 (2011).
95. Hartmann, D. L. *Global Physical Climatology* 2nd edn (Elsevier, 2016).
96. Ashouri, H. et al. PERSIANN-CDR: daily precipitation climate data record from multisatellite observations for hydrological and climate studies. *Bull. Am. Meteor. Soc.* **96**, 69–83 (2015).
97. Lee, H.-T. *Climate Algorithm Theoretical Basis Document (C-ATBD): Outgoing Longwave Radiation (OLR)—Daily* Climate Data Record (CDR) Program Document No. CDRP-ATBD-0526 (NOAA, 2014).

Acknowledgements

Partial support for this research was provided to E.F.-G., J.T.R. and P.S. by the National Science Foundation (NSF) under the TRIPODS+ programme (DMS-1839336). Moreover, the work of E.F.-G. was supported by NSF under the EAGER programme

(grant ECCS-1839441) and by NASA's Global Precipitation Measurement (GPM) programme (grant 80NSSC19K0684). J.T.R. received support from DOE's Office of Science RUBISCO Science Focus Area and NASA's IDS and CMS programmes. J.-Y.Y. and M.S.P. were supported by the NSF Climate and Large-scale Dynamics (CLD) programme under grants AGS-1833075, AGS-173416 and AGS-1912134. The work of P.S., M.S.P., P.A.L. and J.T.R. was also partially supported by NSF under the DGE-1633631 grant. S.Y. was supported by a generous gift to Yale from T. Sandoz. A research grant from UCI to advance these research ideas is also acknowledged. We thank the climate modelling groups around the world for producing and making their model outputs available. We also acknowledge the help from O. Adam and B. Lintner in discussing parts of this analysis.

Author contributions

A.M. designed the study, performed the data analysis, and wrote the first draft of the manuscript. All authors contributed to the conceptualization and interpretation of the results and to extended discussions in the revising and finalizing stages of the manuscript.

Competing interests

The authors declare no competing interests.

Additional information

Supplementary information is available for this paper at https://doi.org/10.1038/s41558-020-00963-x.

Correspondence and requests for materials should be addressed to A.M. or E.F.-G.

Peer review information *Nature Climate Change* thanks Michael Byrne and the other, anonymous, reviewer(s) for their contribution to the peer review of this work.

Reprints and permissions information is available at www.nature.com/reprints.